Stem Cell Reports
Report
OPEN ACCESS

EPHRIN-B1 Mosaicism Drives Cell Segregation in Craniofrontonasal Syndrome hiPSC-Derived Neuroepithelial Cells

Terren K. Niethamer,[1,2,3] Andrew R. Larson,[1,2] Audrey K. O'Neill,[1,2] Marina Bershteyn,[5] Edward C. Hsiao,[1,3,4,6] Ophir D. Klein,[1,3,4,7,8] Jason H. Pomerantz,[1,3,5,8,9] and Jeffrey O. Bush[1,2,3,4,5,*]
[1]Program in Craniofacial Biology
[2]Department of Cell and Tissue Biology
[3]Biomedical Sciences Graduate Program
[4]Institute for Human Genetics
[5]Eli and Edythe Broad Center of Regeneration Medicine and Stem Cell Research
[6]Department of Medicine
[7]Department of Pediatrics
[8]Department of Orofacial Sciences
[9]Division of Plastic and Reconstructive Surgery, Department of Surgery
University of California, San Francisco, San Francisco, CA 94143, USA
*Correspondence: jeffrey.bush@ucsf.edu
http://dx.doi.org/10.1016/j.stemcr.2017.01.017

SUMMARY

Although human induced pluripotent stem cells (hiPSCs) hold great potential for the study of human diseases affecting disparate cell types, they have been underutilized in seeking mechanistic insights into the pathogenesis of congenital craniofacial disorders. Craniofrontonasal syndrome (CFNS) is a rare X-linked disorder caused by mutations in *EFNB1* and characterized by craniofacial, skeletal, and neurological anomalies. Heterozygous females are more severely affected than hemizygous males, a phenomenon termed cellular interference that involves mosaicism for EPHRIN-B1 function. Although the mechanistic basis for cellular interference in CFNS has been hypothesized to involve Eph/ephrin-mediated cell segregation, no direct evidence for this has been demonstrated. Here, by generating hiPSCs from CFNS patients, we demonstrate that mosaicism for EPHRIN-B1 expression induced by random X inactivation in heterozygous females results in robust cell segregation in human neuroepithelial cells, thus supplying experimental evidence that Eph/ephrin-mediated cell segregation is relevant to pathogenesis in human CFNS patients.

INTRODUCTION

Congenital craniofacial disorders represent over one-third of all birth defects (Global strategies to reduce the health care burden of craniofacial anomalies, 2004). While the genetic causes of many syndromes are known, how these mutations lead to abnormal cellular mechanisms underlying these disorders is incompletely understood. A better understanding of the underlying etiology of these disorders is needed to develop new treatment strategies targeted to the cellular and molecular basis of disease. The emergence of human induced pluripotent stem cells (hiPSCs) as a tool for human disease modeling (Takahashi et al., 2007; Takahashi and Yamanaka, 2006; Tiscornia et al., 2011; Yu et al., 2007) holds great promise for improving our cellular understanding of craniofacial diseases, as hiPSCs can be differentiated into patient-specific, disease-relevant cell types. However, perhaps due to the challenge of modeling structural aspects of craniofacial disease in two dimensions in cell culture, hiPSC models for these disorders are not yet widely used.

Craniofrontonasal syndrome (CFNS; OMIM no. 304110) is an X-linked disorder caused by mutations in *EFNB1* and characterized by craniofacial, skeletal, and neurological anomalies (Twigg et al., 2004; Wieland et al., 2004). The most common clinical findings include hypertelorism, frontonasal dysplasia, coronal synostosis, bifid nasal tip, longitudinal splitting of the nails, and wiry or frizzy hair; other less frequent symptoms include cleft lip and palate, diaphragmatic hernia, agenesis of the corpus callosum, syndactyly, and polydactyly (Twigg et al., 2004, 2006, 2013; Wieacker and Wieland, 2005; Wieland et al., 2004). CFNS is an unusual X-linked disorder in that heterozygous females are more severely affected than hemizygous male patients, who are usually unaffected or mildly affected and often present only with hypertelorism (Wieacker and Wieland, 2005). This counterintuitive inversion of severity has been termed cellular interference, a phenomenon whereby random X chromosome inactivation (XCI) in heterozygous female CFNS patients results in mosaicism for *EFNB1* expression, leading to abnormal cellular interactions (Twigg et al., 2013; Wieacker and Wieland, 2005). Consistent with this notion, rare severely affected male CFNS patients have somatic mosaic mutations in *EFNB1* (Twigg et al., 2013), reinforcing mosaicism as an important aspect of CFNS pathogenesis.

EFNB1 encodes EPHRIN-B1, a member of the Eph/ephrin family of membrane-linked signaling molecules, and abnormal signaling between cells expressing wild-type EPHRIN-B1 and cells that are functionally EPHRIN-B1-null

may occur in the mosaic state (Compagni et al., 2003; Wieacker and Wieland, 2005). During development, Eph/ephrin signaling plays an important role in boundary formation, an essential process that requires signaling between adjacent cells and often involves segregation between different cell types (Batlle and Wilkinson, 2012; Cayuso et al., 2015; Fagotto, 2014; Fagotto et al., 2014). Differential expression of Eph receptors and ephrins in vivo can restrict cell intermingling in the vertebrate hindbrain (Xu et al., 1999), limb bud (Compagni et al., 2003; Davy et al., 2004), eye (Cavodeassi et al., 2013), somites (Barrios et al., 2003; Durbin et al., 1998), cranial sutures (Merrill et al., 2006; Ting et al., 2009), and intestinal crypts (Holmberg et al., 2006), as well as in the *Drosophila* wing disc (Umetsu et al., 2014). In culture, expressing an Eph receptor in one population of cells and an ephrin in another restricts intermingling of cells from the two populations (Jorgensen et al., 2009; Mellitzer et al., 1999; Poliakov et al., 2008). Further, cell segregation occurs in developing *Efnb1*$^{+/-}$ mouse limb (Compagni et al., 2003) and secondary palate (Bush and Soriano, 2010), supporting the idea that XCI-induced mosaicism leads to segregation of Ephrin-B1 expressing and non-expressing cells.

The role of Eph/ephrin signaling in boundary formation and supporting data from mouse models suggest that mosaicism for EPHRIN-B1 expression may lead to aberrant cell segregation in human CFNS patients (Compagni et al., 2003; Twigg et al., 2004, 2006, 2013; Wieacker and Wieland, 2005; Wieland et al., 2004). However, it has proven difficult to determine the mechanism of cellular interference, and EPHRIN-B1-mediated cell segregation has not been demonstrated in CFNS patients. Here, we report the generation of an hiPSC model to study defects in morphogenesis in a congenital craniofacial disorder. We demonstrate that cell segregation is a consequence of EPHRIN-B1 mosaicism in CFNS, providing evidence that this cell behavior is relevant to CFNS pathogenesis in humans. The CFNS hiPSC model provides proof of principle that hiPSC-derived cell types can be used both to model structural anomalies and to gain valuable insights into fundamental cellular mechanisms of morphogenesis in patient cells.

RESULTS

Isolation of CFNS Human Dermal Fibroblasts and Reprogramming to hiPSCs

To investigate cellular mechanisms of CFNS, we established human dermal fibroblast (HDF) cultures from a female CFNS patient with a heterozygous mutation in exon 5 of *EFNB1* (*EFNB1*$^{+/c.712delG}$) (Byrne et al., 2009; Hogue et al., 2010). We also established HDF cultures from skin biopsies of the patient's father, a hemizygous carrier of the mutation (*EFNB1*$^{Y/c.712delG}$), and her unaffected mother (*EFNB1*$^{+/+}$). We generated hiPSC lines from low-passage HDFs of each individual using non-integrating episomal vectors (Bershteyn et al., 2014; Okita et al., 2011) and selected three hiPSC lines from each individual for further analysis and experimentation (from the patient, lines CFNShet-1, -2, and -3; from the patient's father, lines CFNShemi-1, -2, and -3; and from the patient's mother, lines wt-1, -2, and -3). Sequencing of exon 5 of *EFNB1* confirmed the expected genotypes (Figures 1A and S1A). All nine hiPSC lines were free of reprogramming plasmid integration by PCR (data not shown) and had normal G-banded karyotypes (Figure S1B).

Characterization of CFNS hiPSC Pluripotency and Differentiation Potential

CFNShet and CFNShemi HDFs were reprogrammed to generate hiPSCs that possessed embryonic stem cell-like morphology similar to that of wild-type hiPSCs. All lines, regardless of genotype, possessed differentiation potential to ectoderm (βIII-tubulin), endoderm (α-fetoprotein), and mesoderm (muscle actin) in an embryoid body protocol (Figures 1B and S1C) and expressed the endogenous pluripotency markers OCT4, SOX2, NANOG, TRA-1-60, and TRA-1-81 (Figures 1C and S1D).

XCI-induced mosaicism in females plays a central role in CFNS (Twigg et al., 2004, 2006, 2013; Wieacker and Wieland, 2005; Wieland et al., 2004). However, XCI status of female hiPSCs can vary across different lines (Lessing et al., 2013), depending on conditions used for reprogramming (Tchieu et al., 2010; Tomoda et al., 2012; Wutz, 2012). To model CFNS, we used reprogramming conditions that favor maintenance of XCI rather than X reactivation (Wutz, 2012) and characterized XCI status of CFNShet HDFs and each CFNShet hiPSC line using the human androgen receptor assay (HUMARA) (Kiedrowski et al., 2011). CFNShet HDFs showed an expected XCI ratio close to 50%, as in earlier studies that indicated no skewed X inactivation in female CFNS patients (Table S1) (Twigg et al., 2004; Wieland et al., 2004, 2007). All three CFNShet hiPSC lines showed complete inactivation of the maternal, wild-type X chromosome, consistent with the clonal XCI expected from female hiPSC lines derived from a single fibroblast under conditions that favor XCI maintenance (Tchieu et al., 2010). Therefore, only the paternal, mutant copy of *EFNB1* is expressed in these lines (Table S1), and they are not expected to express functional EPHRIN-B1.

Differentiation and Characterization of CFNS Neuroepithelial Cells

CFNS affects multiple structures derived from neural crest cells (NCCs), a multipotent population of stem cells that

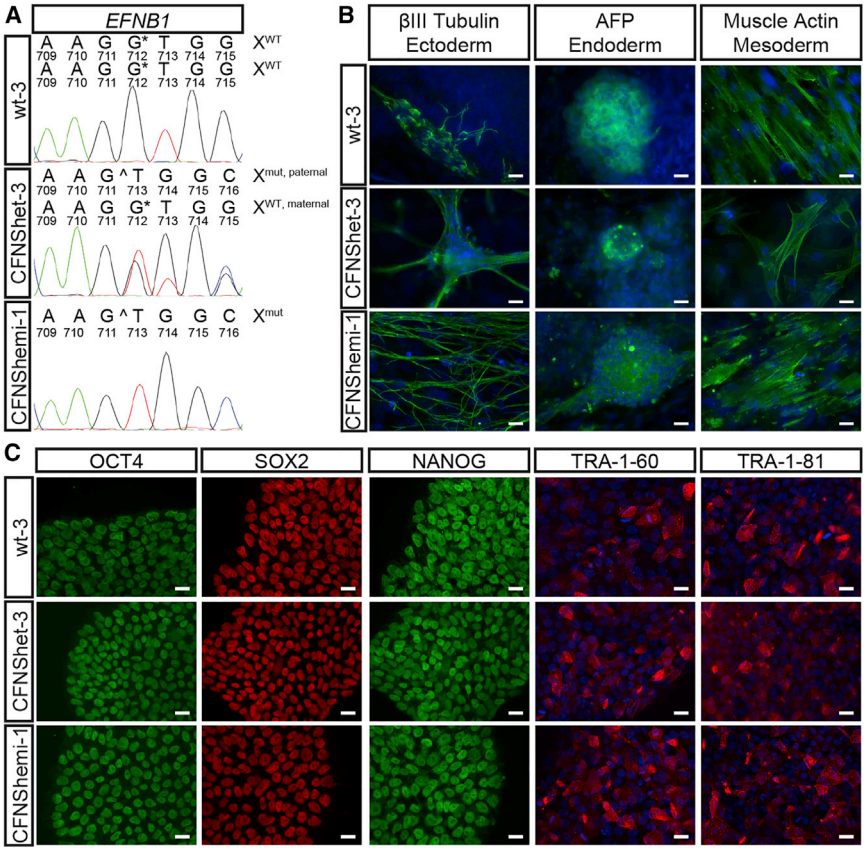

Figure 1. Reprogramming of Wild-Type, CFNShet, and CFNShemi HDFs to hiPSCs

(A) CFNShet-3 and CFNShemi-1 hiPSCs possess the *EFNB1*$^{c.712delG}$ mutation compared with wt-3 hiPSCs. See also Figure S1A.

(B) wt-3, CFNShet-3, and CFNShemi-1 hiPSCs possess differentiation potential to ectoderm (βIII-tubulin), endoderm (α-fetoprotein, AFP), and mesoderm (muscle actin). Samples were counterstained with DAPI (blue). Scale bars, 20 μm. See also Figure S1C.

(C) wt-3, CFNShet-3, and CFNShemi-1 hiPSCs express the endogenous pluripotency markers OCT4, SOX2, NANOG, TRA-1-60, and TRA-1-81. TRA-1-60- and TRA-1-81-labeled samples were counterstained with DAPI (blue). Scale bars, 20 μm. See also Figure S1D.

are induced at the neural plate border, delaminate, and migrate ventrolaterally to populate the craniofacial structures and contribute to skeletal, connective, neural, and vascular tissues. In mice, Ephrin-B1-mediated cell segregation occurs in the NE prior to NCC emigration (O'Neill et al., 2016). We therefore reasoned that NE cells are a good model for testing whether cell segregation occurs in CFNS, and we began by differentiating CFNS and control hiPSCs to human neuroepithelial (hNE) cells. We adapted a monolayer protocol that uses dual-SMAD inhibition to improve neural differentiation efficiency through inhibition of activin and nodal signaling (Chambers et al., 2009). All hNE cells, regardless of genotype, had neuroepithelial morphology and expressed the neural progenitor cell markers PAX6, SOX1, and OTX2 (Figure 2A). These data indicate that CFNS patient hiPSCs are able to differentiate into hNE cells independently of EPHRIN-B1 expression. hNE cells of all genotypes, but not hiPSCs, expressed *EFNB1* mRNA (Figure 2B), and over the course of differentiation to hNE cells, expression of mRNA transcripts of both *EFNB1* and *PAX6* increased in a similar manner in cells of each genotype (Figure 2C). hNE cells of all three genotypes expressed *EFNB2*, a closely related B-type ephrin, as well as *EPHB2* and *EPHB3*, signaling partners of EPHRIN-B1 that are involved in craniofacial development (Orioli et al., 1996) (Figures S2A–S2C). Wild-type hNE cells expressed EPHRIN-B1 protein, whereas CFNShet and CFNShemi *EFNB1* mutant hNE cells did not (Figure 2D).

EPHRIN-B1 Mosaicism Results in Cell Segregation in CFNS hNE Cells

To model *EFNB1* mosaicism and determine whether it results in segregation, we generated mixed cultures of fluorescently labeled hNE cells of different genotypes at a 1:1 ratio (Supplemental Experimental Procedures). Control mixed cultures in which all cells expressed EPHRIN-B1 (wt-3 + wt-3, N = 11/11 trials) or in which no cells expressed EPHRIN-B1 (CFNShet-3 + CFNShet-3, N = 7/7 trials; CFNShemi-1 + CFNShemi-1, N = 4/4 trials) resulted in hNE cells commingling freely, with no notable segregation after 48 hr (Figures 3A–3C). However, in hNE cell populations mosaic for EPHRIN-B1 expression, EPHRIN-B1-expressing cells segregated dramatically from EPHRIN-B1 non-expressing cells, forming distinct boundaries between the two different cell types by 48 hr (Figures 3D and 3E) (wt-3 + CFNShet-3, N = 10/10 trials; wt-3 + CFNShemi-1, N = 4/4 trials). To ensure that this segregation depended

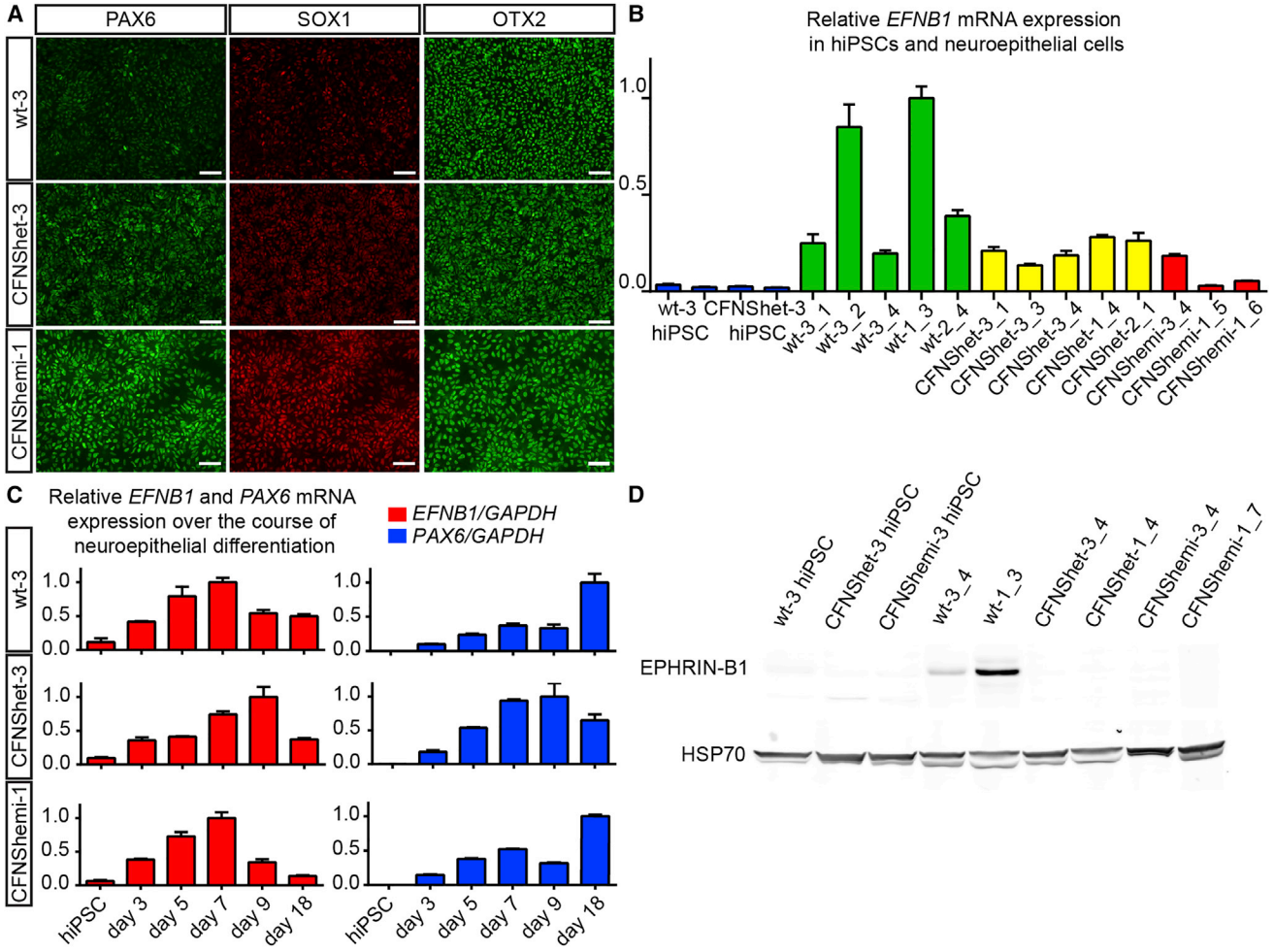

Figure 2. Differentiation and Characterization of hNE Cells from hiPSCs

(A) Immunostaining reveals that wt-3, CFNShet-3, and CFNShemi-1 hNE cells express the hNE cell markers PAX6, SOX1, and OTX2. Scale bars, 50 μm.

(B) *EFNB1* mRNA expression (normalized to *GAPDH* mRNA expression) in hiPSCs and wild-type, CFNShet, and CFNShemi hNE cells. Numbers following underscores represent separate hNE differentiations. Error bars represent the SD of n = 3 technical replicate qRT-PCR reactions per hiPSC or hNE line. See also Figure S2.

(C) Relative *EFNB1* and *PAX6* expression (normalized to *GAPDH* expression) increase over the course of hNE cell differentiation of wt-3, CFNShet-3, and CFNShemi-1 hiPSCs. Error bars represent the SD of n = 3 technical replicate qRT-PCR reactions per condition. Data shown are one of n = 2 biological replicates of each wt-3 and CFNShet-3 or one of n = 3 biological replicates of CFNShemi-1 (n = 2) and CFNShemi-3 (n = 1).

(D) Immunoblotting reveals expression of EPHRIN-B1 protein in wild-type but not CFNShet or CFNShemi hNE cells or in hiPSCs of any genotype.

on EPHRIN-B1 expression and not on differences between independent hNE cell lines, we mixed hNE lines derived from different hiPSC lines of the same genotype and also observed intermixing of cells (wt-3 + wt-2, Figure 3F; CFNShet-3+CFNShet-1, Figure 3G) (N = 3/3 trials, each condition). Further, mixing hNE lines derived from different genotypes lacking EPHRIN-B1 expression (CFNShet-3 + CFNShemi-1, N = 3/3 trials) did not result in cell segregation (Figure 3H), demonstrating that hNE cells segregate based on the presence or absence of EPHRIN-B1 expression and not some other factor associated with individual variability.

To observe the process of cell segregation over time, we used live cell imaging to capture the first 25 hr after cell mixing in both mosaic and EPHRIN-B1 non-expressing cell mixtures. Both cell mixtures were intermingled at time of mixing (t = 0, Figures S3A and S3G). Cells in both mixtures continued to interact with each other over time,

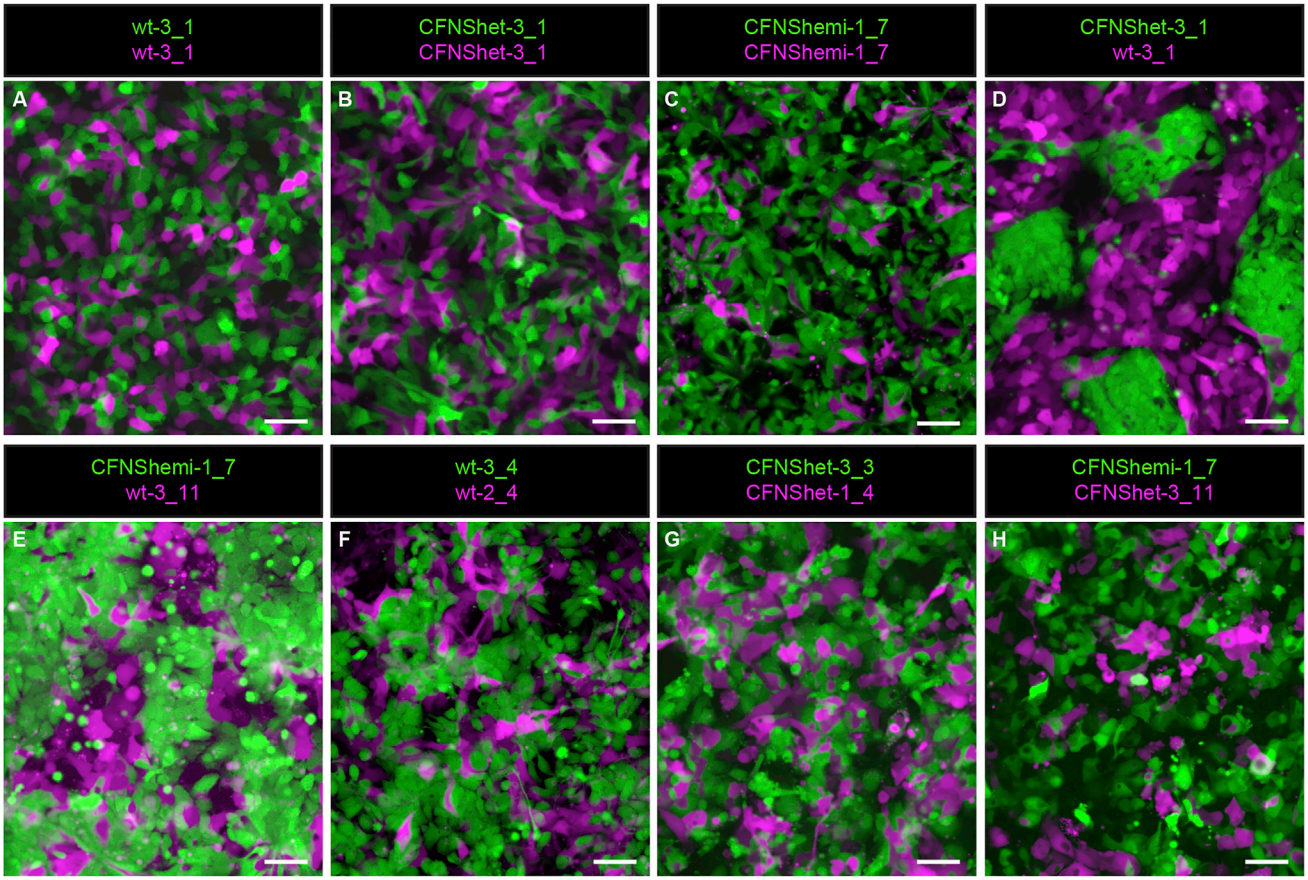

Figure 3. Robust Cell Segregation in Neuroepithelial Cells Mosaic for EPHRIN-B1 Expression

(A–C) Mixing two populations of wild-type EPHRIN-B1 expressing hNE cells (A), two populations of CFNShet hNE cells not expressing EPHRIN-B1 (B), or two populations of CFNShemi hNE cells not expressing EPHRIN-B1 (C) results in cell intermingling over 48 hr.

(D and E) Cell mixing to generate cultures mosaic for EPHRIN-B1 expression (wt-3 + CFNShet-3 (D); wt-3 + CFNShemi-1 (E)) results in robust segregation of EPHRIN-B1 expressing and non-expressing hNE cells over 48 hr. See also Figure S3.

(F–H) Mixing two different wild-type (EPHRIN-B1 expressing) hNE cell lines (wt-3 + wt-2) (F), two different CFNShet (EPHRIN-B1 non-expressing) hNE cell lines (CFNShet-3 + CFNShet-1) (G), or two EPHRIN-B1 non-expressing hNE cell lines of different genotypes (CFNShet-3 + CFNShemi-1) (H) results in cell intermingling without cell segregation. Adjustments to gamma were made to better visualize independent cell populations.

Scale bars, 50 μm.

and EPHRIN-B1 non-expressing mixtures remained freely commingled at each time point (Figures S3B–S3E). However, the EPHRIN-B1 mosaic population of cells segregated progressively over 25 hr (Figures S3H–S3L), indicating that segregation is a continuous process that occurs over time. These data provide evidence that EPHRIN-B1-mediated cell segregation can occur in human CFNS.

DISCUSSION

Here, we have generated an hiPSC model of a human craniofacial condition and have used it to address an outstanding question: does mosaicism for *EFNB1* expression result in cell segregation in human CFNS? The c.712delG mutation found in this CFNS family occurred 5′ to the transmembrane domain-encoding region of *EFNB1*, and we found that *EFNB1* mutant hNE cells did not express EPHRIN-B1, indicating that this mutation results in an unstable EPHRIN-B1 protein and most likely null loss of function. To enable us to model CFNS, it was essential that loss of *EFNB1* function not prevent CFNS patient-derived HDFs from undergoing reprogramming to hiPSCs. We did not observe differences in reprogramming ability between *EFNB1* mutant and control HDFs, leading us to conclude that EPHRIN-B1 expression is not necessary for reprogramming. Further, we found that both control and CFNS hiPSCs possessed differentiation potential to

all three germ layers; loss of EPHRIN-B1 expression does not apparently prevent differentiation. This is consistent with our qRT-PCR data demonstrating that transcripts of *EFNB1* and several other Eph/ephrin signaling family members are expressed at very low levels in hiPSCs relative to hNE cells, suggesting that these signaling molecules may not play critical roles in hiPSCs.

Previous human genetic studies have indicated that mosaicism for *EFNB1* mutation is central to CFNS pathology, a phenomenon termed cellular interference suggested to result in cell segregation based on evidence from model organisms (Compagni et al., 2003; Twigg et al., 2004, 2006, 2013; Wieacker and Wieland, 2005; Wieland et al., 2004). Whether cell segregation occurs in CFNS, however, and in what cell types, was not known. Based on evidence of cell segregation in the neural plate NE in *Efnb1*$^{+/-}$ mice (O'Neill et al., 2016), we differentiated hiPSCs to hNE cells to address this question.

Both wild-type and CFNS patient-derived hNE cells expressed neural stem cell markers and several members of the Eph/ephrin gene family, including *EFNB1*. Expression of *EFNB1* varied between hNE lines, as well as between independent differentiations of the same hiPSC line, indicating that there was inherent variability in the differentiations. Consistently, however, hNE cells expressed higher levels of *EFNB1* than hiPSCs, indicating that increased *EFNB1* expression is a characteristic of the hNE cell type. In addition, *EFNB1* expression decreased as hNE cells were maintained over time, suggesting that higher levels of *EFNB1* expression may mark a progenitor stage in the differentiation program.

As hiPSCs are clonally derived cell lines, CFNShet hNE lines are not mosaic for *EFNB1* expression, necessitating a different approach to model cellular interference. Upon mixing wild-type and EPHRIN-B1 non-expressing hNE cells to generate EPHRIN-B1 mosaicism, the EPHRIN-B1 expressing and non-expressing cells segregated to form ectopic boundaries in culture. This robust segregation occurred in mosaic mixtures of wild-type + CFNShet cells and wild-type + CFNShemi cells, but not in mixtures of two different populations of EPHRIN-B1 expressing cells, or two different populations of EPHRIN-B1 non-expressing cells, even if these two populations were derived from different hiPSC lines. We therefore conclude that segregation is not an effect of mixing different hNE lines, but rather an effect of mosaicism for EPHRIN-B1 expression, and that cellular interference through EPHRIN-B1-mediated cell segregation occurs in CFNS cells. This finding informs our understanding of the etiology of CFNS and indicates that cell segregation contributes to cellular interference. How cell segregation leads to more severe disease phenotypes is not yet clear; the hiPSC model we have developed is a highly relevant system in which to answer remaining questions about CFNS pathology.

An hiPSC model is an important resource because patient cells can be differentiated into multiple disease-relevant cell types, overcoming the challenge of isolating primary cells from patients. It is notable that cell segregation occurs in the neuroepithelium in models of CFNS; recent studies have indicated that Treacher Collins syndrome, another neurocristopathy, also exhibits cellular defects originating in the neuroepithelium and ongoing in the NCC (Jones et al., 2008). Our hiPSC model of CFNS will facilitate further studies of cell segregation, such as investigating whether it occurs in hNCCs and their descendants. This will contribute to a better understanding of the developmental timing of CFNS etiology and will provide the ability to study aspects of the disease that are less well understood. For example, mutations in *EFNB1* that cause CFNS are responsible for approximately 7% of cases of craniosynostosis in which a genetic cause is known (Johnson and Wilkie, 2011), and studies in mice have demonstrated that suture boundary formation is regulated by A-type Eph/ephrin signaling (Merrill et al., 2006; Ting et al., 2009). However, how EPHRIN-B1 affects boundary formation and maintenance at the suture is unknown, because *EFNB1* mutant mice do not exhibit craniosynostosis. Further, in CFNS, other organ systems not derived from NCCs are also affected; patients exhibit limb anomalies and defects of the axial skeleton that may be attributable to cell segregation (Compagni et al., 2003; Davy et al., 2004, 2006). Differentiation of hiPSCs into these various cell types is a method for testing the importance of EPH/EPHRIN-mediated cell segregation in various tissues.

hiPSC models of congenital craniofacial disease will also facilitate targeted molecular therapies for these disorders. As we have shown that cell segregation resulting from EPHRIN-B1 mosaicism occurs in human CFNS cells, therapeutic benefits may be derived from preventing segregation. Additional research to determine the mechanism by which hNE cell segregation leads to craniofacial phenotypes in CFNS patients is likely to identify molecular candidates that could be targeted to achieve this goal. A human model system of EPHRIN-B1-mediated cell segregation could then serve as a high-throughput system for testing candidate therapeutic molecules. Finally, this CFNS hiPSC model system may encourage the use of hiPSC-based systems to model structural aspects of other congenital craniofacial anomalies in which self-organization of cells may play a role. Such studies have the potential to inform therapeutic approaches for congenital craniofacial anomalies, as well as to increase our understanding of cell self-organizing properties to facilitate tissue engineering and cell replacement therapies for patients with these disorders.

EXPERIMENTAL PROCEDURES

hiPSC Generation, Culture, and Characterization

All human tissue collection, stem cell studies, procedures, and written consents were approved by the University of California, San Francisco (UCSF) Committee on Human Research and the UCSF Gamete, Embryo, and Stem Cell Research Committee. Prior to their inclusion in this study, written informed consent was obtained from all participants or from their parents. CFNS and control hiPSCs were established from primary human fibroblast cultures from each subject (Byrne et al., 2009) using episomal reprogramming (Bershteyn et al., 2014; Okita et al., 2011). hiPSC lines were genetically characterized using G-banded karyotype analysis (WiCell Research Institute) and sequencing of *EFNB1* (SeqWright). hiPSCs were also assayed for episomal plasmid integration and for relative inactivation of each X chromosome with the HUMAR assay (Kiedrowski et al., 2011). See also the Supplemental Experimental Procedures.

hNE Cell Differentiation

Neural inductions were performed using a modified monolayer dual-SMAD inhibition protocol (Chambers et al., 2009) with STEMdiff Neural Induction Medium (STEMCELL Technologies) containing 10 μM SB-431542 (Santa Cruz Biotechnology) and 5 μM DMH1 (Sigma). See also the Supplemental Experimental Procedures.

Immunocytochemistry and Immunoblotting

For immunocytochemistry, cells were plated on Matrigel-coated glass coverslips. For immunoblotting, cells were lysed in NP-40 lysis buffer containing protease and phosphatase inhibitors. Both procedures were performed using standard protocols. See also the Supplemental Experimental Procedures.

qRT-PCR of hiPSCs and Neuroepithelial Cells

Total RNA was extracted from cells using TRIzol (Life Technologies). RNA was reverse transcribed using a SuperScript II First-Strand Synthesis System for RT-PCR (Life Technologies). qRT-PCR was performed using iTaq Universal SYBR Green and a CFX96 Real Time System (Bio-Rad), with primer pairs that span exon-intron boundaries (see Supplemental Experimental Procedures for primer sequences).

Statistics

For analysis of qRT-PCR data, GraphPad Prism 6 was used to plot mean expression ± SD of technical replicate reactions, indicated by error bars. Biological replicates (different hiPSC lines or different hNE differentiations), if applicable, are shown as separate bars on the graph.

SUPPLEMENTAL INFORMATION

Supplemental Information includes Supplemental Experimental Procedures, three figures, and one table and can be found with this article online at http://dx.doi.org/10.1016/j.stemcr.2017.01.017.

AUTHOR CONTRIBUTIONS

T.K.N., A.R.L., and J.O.B. designed experiments and analyzed data. O.D.K. and J.H.P. obtained patient material for generation of hiPSCs. A.R.L. and J.O.B. made and characterized hiPSC lines with technical expertise from E.C.H. T.K.N. differentiated, characterized, and performed experiments on hiPSC-derived neuroepithelial cells with technical expertise from M.B. and A.K.O. T.K.N. and J.O.B. wrote the manuscript.

ACKNOWLEDGMENTS

This study was supported by a Graduate Research Fellowship (2013157314) to T.K.N. from the National Science Foundation, and by grant F31DE026059 to T.K.N., and grant R01DE02337 to J.O.B., both from the National Institute of Dental and Craniofacial Research. A.R.L. was a Howard Hughes Medical Institute Medical Research Fellow and completed this work as partial fulfillment of the requirements for an M.D. with Distinction in the UCSF Molecular Medicine Pathway to Discovery. Any opinions, findings, or conclusions in this work are those of the authors and do not necessarily reflect the views of the Howard Hughes Medical Institute, National Science Foundation, or NIH.

Received: August 10, 2016
Revised: January 17, 2017
Accepted: January 18, 2017
Published: February 23, 2017

REFERENCES

Barrios, A., Poole, R.J., Durbin, L., Brennan, C., Holder, N., and Wilson, S.W. (2003). Eph/Ephrin signaling regulates the mesenchymal-to-epithelial transition of the paraxial mesoderm during somite morphogenesis. Curr. Biol. *13*, 1571–1582.

Batlle, E., and Wilkinson, D.G. (2012). Molecular mechanisms of cell segregation and boundary formation in development and tumorigenesis. Cold Spring Harb. Perspect. Biol. *4*, a008227.

Bershteyn, M., Hayashi, Y., Desachy, G., Hsiao, E.C., Sami, S., Tsang, K.M., Weiss, L.A., Kriegstein, A.R., Yamanaka, S., and Wynshaw-Boris, A. (2014). Cell-autonomous correction of ring chromosomes in human induced pluripotent stem cells. Nature *507*, 99–103.

Bush, J.O., and Soriano, P. (2010). Ephrin-B1 forward signaling regulates craniofacial morphogenesis by controlling cell proliferation across Eph-ephrin boundaries. Genes Dev. *24*, 2068–2080.

Byrne, J.A., Nguyen, H.N., and Reijo Pera, R.A. (2009). Enhanced generation of induced pluripotent stem cells from a subpopulation of human fibroblasts. PLoS One *4*, e7118.

Cavodeassi, F., Ivanovitch, K., and Wilson, S.W. (2013). Eph/Ephrin signalling maintains eye field segregation from adjacent neural plate territories during forebrain morphogenesis. Dev. Camb. Engl. *140*, 4193–4202.

Cayuso, J., Xu, Q., and Wilkinson, D.G. (2015). Mechanisms of boundary formation by Eph receptor and ephrin signaling. Dev. Biol. *401*, 122–131.

Chambers, S.M., Fasano, C.A., Papapetrou, E.P., Tomishima, M., Sadelain, M., and Studer, L. (2009). Highly efficient neural conversion of human ES and iPS cells by dual inhibition of SMAD signaling. Nat. Biotechnol. *27*, 275–280.

Compagni, A., Logan, M., Klein, R., and Adams, R.H. (2003). Control of skeletal patterning by ephrinB1-EphB interactions. Dev. Cell *5*, 217–230.

Davy, A., Aubin, J., and Soriano, P. (2004). Ephrin-B1 forward and reverse signaling are required during mouse development. Genes Dev. *18*, 572–583.

Davy, A., Bush, J.O., and Soriano, P. (2006). Inhibition of gap junction communication at ectopic Eph/ephrin boundaries underlies craniofrontonasal syndrome. PLoS Biol. *4*, e315.

Durbin, L., Brennan, C., Shiomi, K., Cooke, J., Barrios, A., Shanmugalingam, S., Guthrie, B., Lindberg, R., and Holder, N. (1998). Eph signaling is required for segmentation and differentiation of the somites. Genes Dev. *12*, 3096–3109.

Fagotto, F. (2014). The cellular basis of tissue separation. Development *141*, 3303–3318.

Fagotto, F., Winklbauer, R., and Rohani, N. (2014). Ephrin-Eph signaling in embryonic tissue separation. Cell Adh. Migr. *8*, 308–326.

Global strategies to reduce the health care burden of craniofacial anomalies: report of WHO meetings on international collaborative research on craniofacial anomalies. Cleft Palate Craniofac. J. *41*, 238–243.

Hogue, J., Shankar, S., Perry, H., Patel, R., Vargervik, K., and Slavotinek, A. (2010). A novel *EFNB1* mutation (c.712delG) in a family with craniofrontonasal syndrome and diaphragmatic hernia. Am. J. Med. Genet. A. *152A*, 2574–2577.

Holmberg, J., Genander, M., Halford, M.M., Annerén, C., Sondell, M., Chumley, M.J., Silvany, R.E., Henkemeyer, M., and Frisén, J. (2006). EphB receptors coordinate migration and proliferation in the intestinal stem cell niche. Cell *125*, 1151–1163.

Johnson, D., and Wilkie, A.O.M. (2011). Craniosynostosis. Eur. J. Hum. Genet. *19*, 369–376.

Jones, N.C., Lynn, M.L., Gaudenz, K., Sakai, D., Aoto, K., Rey, J.-P., Glynn, E.F., Ellington, L., Du, C., Dixon, J., et al. (2008). Prevention of the neurocristopathy Treacher Collins syndrome through inhibition of p53 function. Nat. Med. *14*, 125–133.

Jorgensen, C., Sherman, A., Chen, G.I., Pasculescu, A., Poliakov, A., Hsiung, M., Larsen, B., Wilkinson, D.G., Linding, R., and Pawson, T. (2009). Cell-specific information processing in segregating populations of Eph receptor ephrin-expressing cells. Science *326*, 1502–1509.

Kiedrowski, L.A., Raca, G., Laffin, J.J., Nisler, B.S., Leonhard, K., McIntire, E., and Mongomery, K.D. (2011). DNA methylation assay for X-chromosome inactivation in female human iPS Cells. Stem Cell Rev. Rep. *7*, 969–975.

Lessing, D., Anguera, M.C., and Lee, J.T. (2013). X chromosome inactivation and epigenetic responses to cellular reprogramming. Annu. Rev. Genomics Hum. Genet. *14*, 85–110.

Mellitzer, G., Xu, Q., and Wilkinson, D.G. (1999). Eph receptors and ephrins restrict cell intermingling and communication. Nature *400*, 77–81.

Merrill, A.E., Bochukova, E.G., Brugger, S.M., Ishii, M., Pilz, D.T., Wall, S.A., Lyons, K.M., Wilkie, A.O.M., and Maxson, R.E. (2006). Cell mixing at a neural crest-mesoderm boundary and deficient ephrin-Eph signaling in the pathogenesis of craniosynostosis. Hum. Mol. Genet. *15*, 1319–1328.

Okita, K., Matsumura, Y., Sato, Y., Okada, A., Morizane, A., Okamoto, S., Hong, H., Nakagawa, M., Tanabe, K., Tezuka, K., et al. (2011). A more efficient method to generate integration-free human iPS cells. Nat. Methods *8*, 409–412.

O'Neill, A.K., Kindberg, A.A., Niethamer, T.K., Larson, A.R., Ho, H.H., Greenberg, M.E., and Bush, J.O. (2016). Unidirectional Eph/ephrin signaling creates a cortical actin differential to drive cell segregation. J. Cell Biol. *215*, 217–229.

Orioli, D., Henkemeyer, M., Lemke, G., Klein, R., and Pawson, T. (1996). Sek4 and Nuk receptors cooperate in guidance of commissural axons and in palate formation. EMBO J. *15*, 6035–6049.

Poliakov, A., Cotrina, M.L., Pasini, A., and Wilkinson, D.G. (2008). Regulation of EphB2 activation and cell repulsion by feedback control of the MAPK pathway. J. Cell Biol. *183*, 933–947.

Takahashi, K., and Yamanaka, S. (2006). Induction of pluripotent stem cells from mouse embryonic and adult fibroblast cultures by defined factors. Cell *126*, 663–676.

Takahashi, K., Tanabe, K., Ohnuki, M., Narita, M., Ichisaka, T., Tomoda, K., and Yamanaka, S. (2007). Induction of pluripotent stem cells from adult human fibroblasts by defined factors. Cell *131*, 861–872.

Tchieu, J., Kuoy, E., Chin, M.H., Trinh, H., Patterson, M., Sherman, S.P., Aimiuwu, O., Lindgren, A., Hakimian, S., Zack, J.A., et al. (2010). Female human iPSCs retain an inactive X chromosome. Cell Stem Cell *7*, 329–342.

Ting, M.-C., Wu, N.L., Roybal, P.G., Sun, J., Liu, L., Yen, Y., and Maxson, R.E. (2009). EphA4 as an effector of Twist1 in the guidance of osteogenic precursor cells during calvarial bone growth and in craniosynostosis. Development *136*, 855–864.

Tiscornia, G., Vivas, E.L., and Izpisúa Belmonte, J.C. (2011). Diseases in a dish: modeling human genetic disorders using induced pluripotent cells. Nat. Med. *17*, 1570–1576.

Tomoda, K., Takahashi, K., Leung, K., Okada, A., Narita, M., Yamada, N.A., Eilertson, K.E., Tsang, P., Baba, S., White, M.P., et al. (2012). Derivation conditions impact X-inactivation status in female human induced pluripotent stem cells. Cell Stem Cell *11*, 91–99.

Twigg, S.R., Kan, R., Babbs, C., Bochukova, E.G., Robertson, S.P., Wall, S.A., Morriss-Kay, G.M., and Wilkie, A.O. (2004). Mutations of ephrin-B1 (*EFNB1*), a marker of tissue boundary formation, cause craniofrontonasal syndrome. Proc. Natl. Acad. Sci. USA *101*, 8652–8657.

Twigg, S.R.F., Matsumoto, K., Kidd, A.M.J., Goriely, A., Taylor, I.B., Fisher, R.B., Hoogeboom, A.J.M., Mathijssen, I.M.J., Lourenço, M.T., Morton, J.E.V., et al. (2006). The origin of *EFNB1* mutations in craniofrontonasal syndrome: frequent somatic mosaicism and explanation of the paucity of carrier males. Am. J. Hum. Genet. *78*, 999–1010.

Twigg, S.R.F., Babbs, C., van den Elzen, M.E.P., Goriely, A., Taylor, S., McGowan, S.J., Giannoulatou, E., Lonie, L., Ragoussis, J.,

Akha, E.S., et al. (2013). Cellular interference in craniofrontonasal syndrome: males mosaic for mutations in the X-linked *EFNB1* gene are more severely affected than true hemizygotes. Hum. Mol. Genet. *22*, 1654–1662.

Umetsu, D., Dunst, S., and Dahmann, C. (2014). An RNA interference screen for genes required to shape the anteroposterior compartment boundary in *Drosophila* identifies the Eph receptor. PLoS One *9*, e114340.

Wieacker, P., and Wieland, I. (2005). Clinical and genetic aspects of craniofrontonasal syndrome: towards resolving a genetic paradox. Mol. Genet. Metab. *86*, 110–116.

Wieland, I., Jakubiczka, S., Muschke, P., Cohen, M., Thiele, H., Gerlach, K.L., Adams, R.H., and Wieacker, P. (2004). Mutations of the Ephrin-B1 gene cause craniofrontonasal syndrome. Am. J. Hum. Genet. *74*, 1209–1215.

Wieland, I., Makarov, R., Reardon, W., Tinschert, S., Goldenberg, A., Thierry, P., and Wieacker, P. (2007). Dissecting the molecular mechanisms in craniofrontonasal syndrome: differential mRNA expression of mutant *EFNB1* and the cellular mosaic. Eur. J. Hum. Genet. *16*, 184–191.

Wutz, A. (2012). Epigenetic alterations in human pluripotent stem cells: a tale of two cultures. Cell Stem Cell *11*, 9–15.

Xu, Q., Mellitzer, G., Robinson, V., and Wilkinson, D.G. (1999). In vivo cell sorting in complementary segmental domains mediated by Eph receptors and ephrins. Nature *399*, 267–271.

Yu, J., Vodyanik, M.A., Smuga-Otto, K., Antosiewicz-Bourget, J., Frane, J.L., Tian, S., Nie, J., Jonsdottir, G.A., Ruotti, V., Stewart, R., et al. (2007). Induced pluripotent stem cell lines derived from human somatic cells. Science *318*, 1917–1920.

Stem Cell Reports, Volume *8*

Supplemental Information

EPHRIN-B1 Mosaicism Drives Cell Segregation in Craniofrontonasal Syndrome hiPSC-Derived Neuroepithelial Cells

Terren K. Niethamer, Andrew R. Larson, Audrey K. O'Neill, Marina Bershteyn, Edward C. Hsiao, Ophir D. Klein, Jason H. Pomerantz, and Jeffrey O. Bush

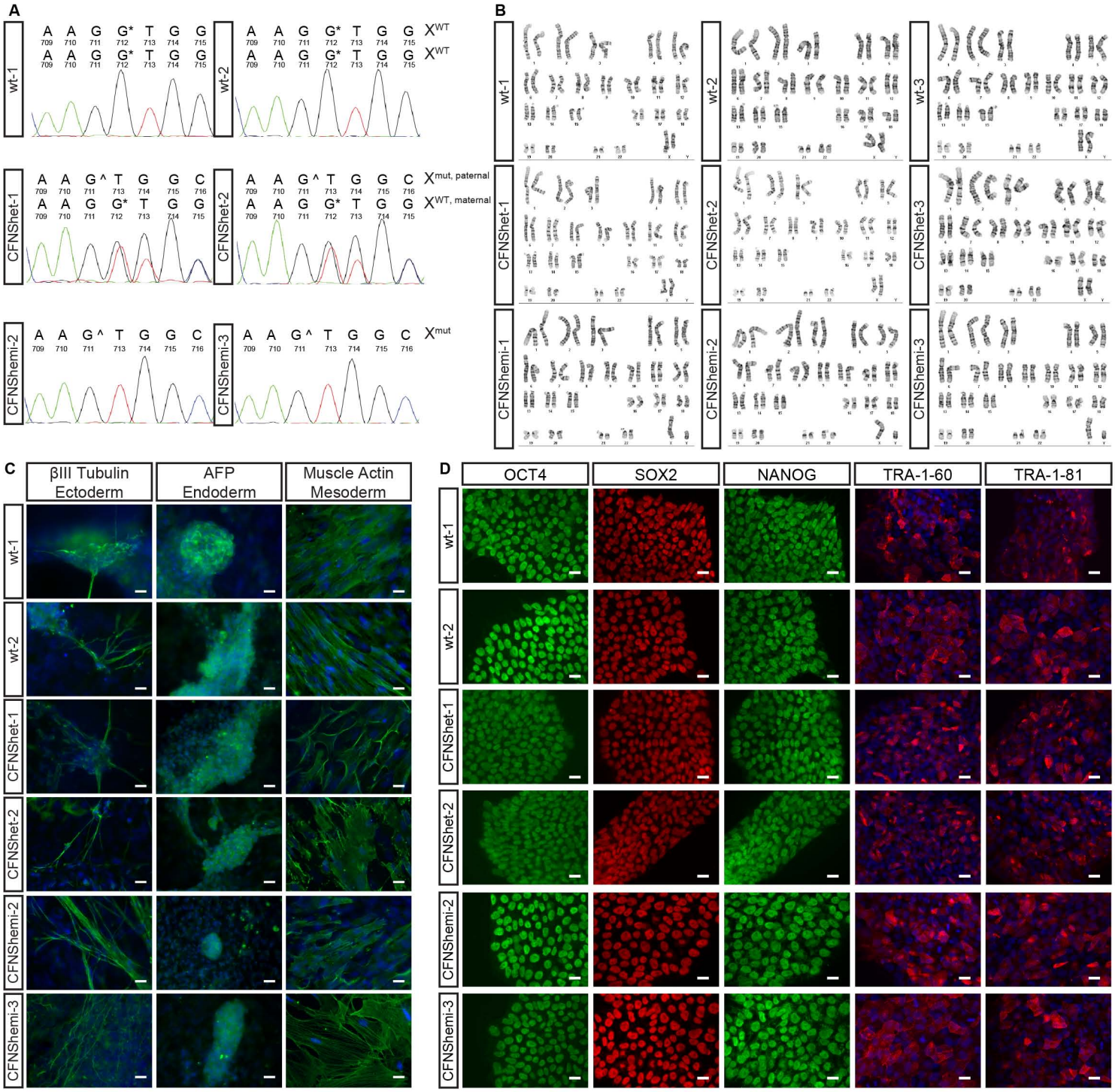

Figure S1. ***Related to Figure 1.*** **Characterization of CFNS patient-derived hiPSCs. (A)** Sequencing chromatograms show retention of G712 in wt hiPSC lines, heterozygous deletion of G712 in CFNShet lines, and deletion of G712 in CFNShemi lines. **(B)** G-banded karyotype analysis shows that all nine hiPSC lines have normal karyotypes (46, XX for female wild type and CFNS heterozygous lines and 46, XY for male CFNS hemizygous lines). **(C)** Upon in vitro embryoid body differentiation, *EFNB1*$^{+/+}$ lines (wt-1, -2), *EFNB1*$^{+/c.712delG}$ lines (CFNShet-1, -2), and *EFNB1*$^{Y/c.712delG}$ lines (CFNShemi-2, -3) demonstrated differentiation potential to ectoderm (βIII tubulin), endoderm (alpha-fetoprotein, AFP), and mesoderm (muscle actin). Samples were counterstained with DAPI (blue). Scale bars, 20 µm. **(D)** Immunocytochemical characterization of *EFNB1*$^{+/+}$ lines (wt-1, -2), *EFNB1*$^{+/c.712delG}$ lines (CFNShet-1, -2), and *EFNB1*$^{Y/c.712delG}$ lines (CFNShemi-2, -3) reveals positive staining for the nuclear factors OCT4, SOX2, and NANOG, as well as the surface antigens TRA-1-60 and TRA-1-81 (counterstained with DAPI (blue)). Scale bars, 20 µm.

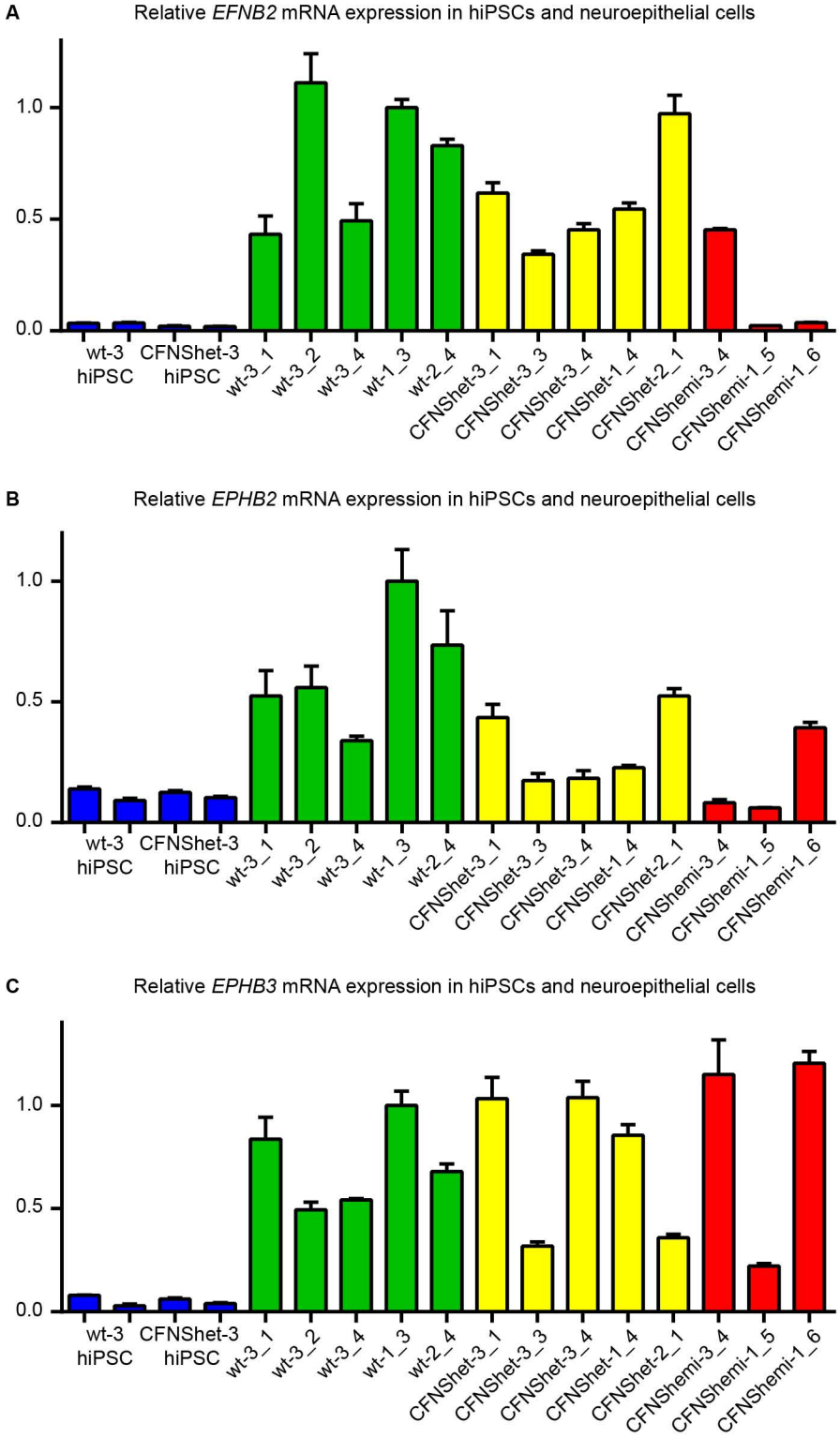

Figure S2. ***Related to Figure 2.*** **Expression of additional EphB/ephrinB signaling family members in hiPSCs and hNE.** qRT-PCR demonstrates expression levels of **(A)** *EFNB2*, **(B)** *EPHB2*, and **(C)** *EPHB3* in hNE cells of all three genotypes. Very low expression of each of these Eph/ephrin signaling family members is seen in hiPSCs. Expression of each Eph/ephrin signaling family member in each sample was normalized to expression of GAPDH. Error bars represent the standard deviation of three technical replicates per hiPSC or hNE line.

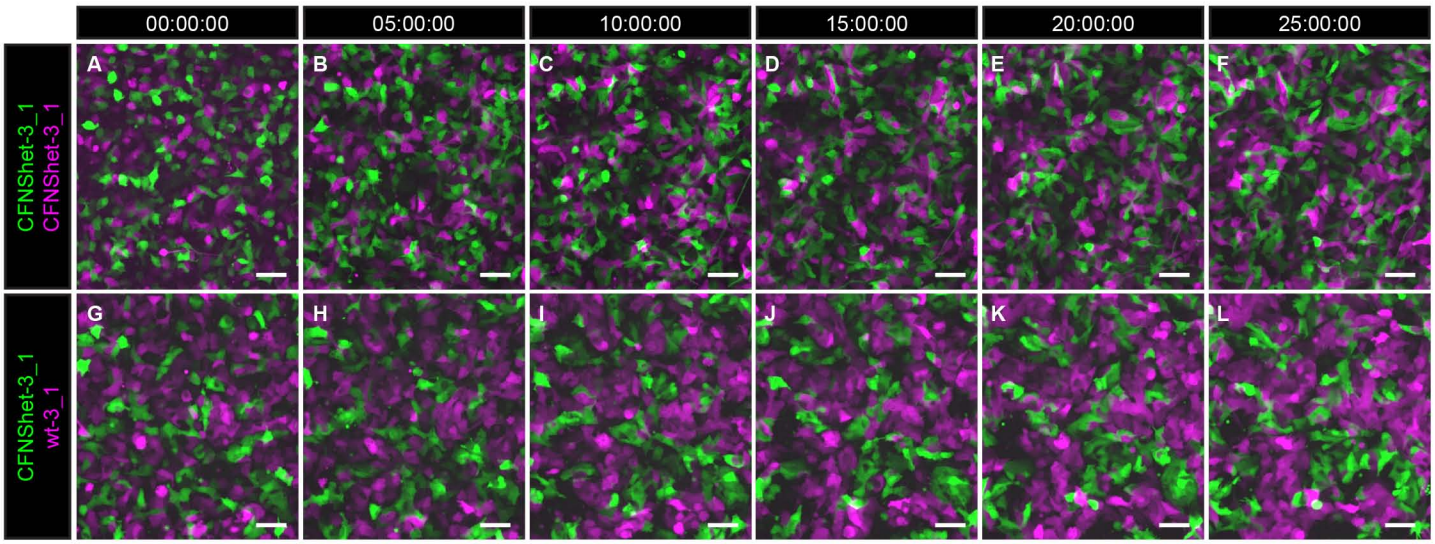

Figure S3. ***Related to Figure 3.*** **Live imaging of hNE cell mixing experiments. (A-F)** Live imaging of a mixture of EPHRIN-B1 non-expressing cells (CFNShet-3+CFNShet-3) over 25 hours demonstrates that EPHRIN-B1 non-expressing cells remain intermixed as they continue to interact with each other, and are not segregating at 25 hours **(F)**. **(G-L)** Live imaging of a cell mixture mosaic for EPHRIN-B1 expression (CFNShet-3+wt-3) shows that cells are intermixed at the beginning of the experiment **(G)**, but segregate from each other over time, and are already forming patches of EPHRIN-B1 expressing and non-expressing cells at 25 hours **(L)**. Scale bars, 50 μm.

Table S1. ***Related to Figure 1.*** **HUMARA demonstrates clonal inactivation of maternal (wild type) X chromosome in each CFNShet hiPSC line.**

	Peak Areas Undigested Samples		**Peak Areas** Digested Samples		**Possible Values of X_A** (Fraction of X activation)		**Ratio of X_A^{wt} to X_A^{mut}** (Average % X activation)	
	Maternal	Paternal	Maternal	Paternal	X_A, maternal	X_A, paternal	X_A, maternal	X_A, paternal
CFNShet HDFs	64276	61770	9880	19316	0.65	0.35	61	39
	51069	43431	16592	24562	0.56	0.44		
					0.63	0.37		
					0.58	0.42		
CFNShet-1 hiPSCs	59768	205805	28403	0	0.00	1.00	0	100
	17428	57018	4606	0	0.00	1.00		
					0.00	1.00		
					0.00	1.00		
CFNShet-2 hiPSCs	69895	230728	183006	0	0.00	1.00	0	100
	41823	157233	173086	0	0.00	1.00		
					0.00	1.00		
					0.00	1.00		
CFNShet-3 hiPSCs	50731	158352	42899	0	0.00	1.00	0	100
	53890	163248	94864	0	0.00	1.00		
					0.00	1.00		
					0.00	1.00		

Supplemental Experimental Procedures

hiPSC generation and culture. A small dermal tissue sample was collected from an excess specimen at the time of a surgical procedure of the 10-month-old female CFNS proband. Punch biopsies were obtained from the proband's father and mother. Primary human fibroblast cultures were established and cultured on plastic culture dishes in DMEM high glucose (Life Technologies) containing 10% FBS (HyClone), 2 mM L-glutamine, 1 mM sodium pyruvate, 0.1 mM MEM non-essential amino acids, and penicillin-streptomycin-fungizone. Human iPSCs were generated using episomal reprogramming (Bershteyn et al., 2014; Okita et al., 2011). Briefly, one microgram of each of the Y4 combination of episomal reprogramming factors (Addgene 27078, 27080, 27082) was electroporated into 3 $x10^5$ fibroblasts (passage 5-6) with the Neon Electroporation Device (Invitrogen) using the 100-uL kit and conditions of 1650 V, 10 ms, and three pulses. Cells were detached 6 days after electroporation and seeded at 1.5 x 10^5 cells per 10-cm dish onto irradiated mouse embryonic fibroblasts (Globalstem). On day 7, media was changed from fibroblast media to KnockOut™ ESC/hiPSC culture media containing 4 ng/mL bFGF (Life Technologies), and cells were cultured for a further 18-25 days. Colonies with hiPSC-like morphology were manually selected under a dissecting microscope and subcultured on irradiated MEFs. By passage four, hiPSCs were transferred to feeder-free conditions and cultured in mTeSR1 medium (STEMCELL Technologies) on dishes coated with hESC-qualified Matrigel (Corning).

hiPSC characterization. G-banded karyotype analysis of hiPSC lines was performed after passage 9 by WiCell Research Institute (Madison, WI). To confirm *EFNB1* genotypes, DNA samples were isolated from both HDF and hiPSC lines with a DNeasy Blood and Tissue Kit (Qiagen) and sequenced by SeqWright, Inc. (Houston, TX). To assay for plasmid integration, DNA samples were amplified by PCR with *EBNA-1* plasmid backbone-specific primers and normalized to *GAPDH* as a loading control (see below for primer information). PCR products were resolved against a positive control plasmid diluted to the equivalent of 1 and 0.2 copies plasmid/diploid genome. Female HDF and hiPSC cultures were assayed for relative inactivation of each X-chromosome with the HUMAR assay (Kiedrowski et al., 2011). Briefly, capillary electrophoresis was performed on genomic DNA samples both digested and undigested with the methylation-sensitive restriction enzyme HpaII, which selectively digests the active X chromosome. Each allele is represented as a separate peak in the capillary electrophoresis trace based on the differential number of CAG repeats at the human androgen receptor locus on each X-chromosome. Areas under the peak for each allele were measured on Peak Scanner™ (Applied Biosystems) for both undigested and digested samples, and these peak areas were used to calculate X_A (fraction of expression from a given X chromosome).

hNE cell differentiation and culture. hNE cell differentiations from hiPSCs were performed using a monolayer dual-SMAD inhibition protocol (Chambers et al., 2009), with some modifications. hiPSCs were plated on hESC-qualified Matrigel (Corning)-coated dishes at a density of 2.5 x 10^5 cells/cm^2 (day 0) in STEMdiff Neural Induction Medium (NIM; STEMCELL Technologies) supplemented with penicillin-streptomycin (P/S) and 10 μM Y-27632 (Santa Cruz Biotechnology) to increase cell survival as single cells (Watanabe et al., 2007). Daily media changes were made with NIM supplemented with P/S, 10 μM SB-431542 (Santa Cruz Biotechnology), and 5 μM DMH1 (Sigma) (Neely et al., 2012) on days 1-3 and NIM + P/S alone on days 4 onward. After 8-10 days in culture, cells were dissociated to a single-cell suspension in Accutase and replated on Matrigel-coated dishes at a 1:1 dilution in NIM supplemented with P/S and 10 μM Y-27632. hNE cell cultures were maintained in NIM with or without SB-431542 and DMH1 and split at ratios of 1:1 to 1:3 until experimentation.

hNE cell segregation assays. EPHRIN-B1-expressing and EPHRIN-B1-non-expressing hNE cells were either labeled with CellTracker dye CMFDA (Molecular Probes) for 45 minutes at a concentration of 5μM in NIM supplemented with penicillin-streptomycin (P/S) or infected with adenovirus Ad-CMV-eGFP or Ad-CMV-mCherry (Vector Biolabs) overnight at a concentration of 1-5 x 10^6 IFU/cm^2 in NIM + P/S, followed by incubation in NIM + P/S for 2 additional days. hNE cells from differentially labeled lines were mixed at a concentration of 5 x 10^5 cells/line and plated on Matrigel-coated 24-well glass-bottom dishes (MatTek), for a total of 1 x 10^6 cells per well. Cells were imaged at 48 hours after mixing on a Zeiss Cell Observer spinning disc confocal microscope to assess cell segregation. For live imaging of cell segregation, cell mixing experiments were set up as described above and plated in 4-chamber glass-bottom dishes (Greiner Bio-One), with cell number adjusted to achieve the same density. 15 mM HEPES (UCSF Cell Culture Facility) was added to cell media to facilitate buffering outside the CO_2 incubator during the imaging process. Cell mixtures were imaged at twenty minute intervals over 25 hours after mixing using a Zeiss Cell Observer spinning disc confocal microscope.

Immunocytochemistry. Cells were plated on Matrigel-coated glass coverslips and fixed in 2% paraformaldehyde in PBS at room temperature. The cells were washed with PBS, blocked in 5% normal donkey serum (Jackson ImmunoResearch) and 0.1% Triton-X-100 in PBS, incubated in primary antibody for 1 hour at room temperature or overnight at 4°C, washed with PBS, and incubated in secondary antibody at room temperature (see below for antibody information). Cells were counterstained in 0.1 μg/mL DAPI (Millipore) in PBS for 20 minutes at room temperature and mounted on slides using Aquamount (Thermo Scientific) for imaging.

Immunoblotting. Cells were lysed in NP-40 lysis buffer (20 mM Tris-HCl, 137 mM NaCl, 10% glycerol, 1% NP-40, 2 mM EDTA) supplemented with 1 mM dithiothreitol (Sigma) and the following protease and phosphatase inhibitors: aprotinin, 2 μg/mL; leupeptin, 5 μg/mL; pepstatin, 1 μg/mL; PMSF, 1 mM; NaF, 10 mM; and $NaVO_4$, 1 mM. Protein quantification was performed using the Pierce BCA Protein Assay Kit (Thermo Fisher Scientific). Immunoblotting was performed according to standard procedures using Odyssey® TBS blocking buffer (LI-COR) for blocking and dilution of antibodies (see below for antibody information) and TBS with 0.1%

Tween-20 for washing. Imaging of immunoblots was performed using an Odyssey® Infrared Imaging System (LI-COR), and analysis was carried out using Image Studio™ software (LI-COR).

Antibody Information

ICC - Conjugated Antibodies	Source	Catalog #	Dilution
TRA-1-60, Cy3 conjugate	Millipore	MAB4360C3	1:100
TRA-1-81, Cy3 conjugate	Millipore	MAB4381C3	1:100
NANOG, Alexa Fluor 488 conjugate	Millipore	MABD24A4	1:100
SOX2, Cy3 conjugate	Millipore	MAB4423C3	1:100
OCT4 (POU5FL), Alexa Fluor 488 conjugate	Millipore	MAB4419A4	1:100
ICC - Primary Antibodies	**Source**	**Catalog #**	**Dilution**
βIII-tubulin (TUJ1)	Sigma	T8660	1:1000
α-fetoprotein (AFP)	Sigma	A8452	1:500
human muscle actin	DAKO	M0635	1:50
SOX1	R&D Systems	AF3369	1:150
PAX6	Covance	PRB-278P	1:200
OTX2	Millipore	AB9566	1:250
ICC - Secondary Antibodies	**Source**	**Catalog #**	**Dilution**
Donkey anti-rabbit Alexa Fluor 488	Jackson ImmunoResearch	711-165-152	1:400
Donkey anti-mouse Cy2	Jackson ImmunoResearch	715-225-150	1:400
Donkey anti-goat Cy3	Jackson ImmunoResearch	705-165-003	1:400
IB - Primary Antibodies	**Source**	**Catalog #**	**Dilution**
EPHRIN-B1	R&D Systems	AF473	0.2 μg/mL
HSP70	BD Transduction	610607	1:1000
IB - Secondary Antibodies	**Source**	**Catalog #**	**Dilution**
Donkey anti-goat IRDye® 800CW	LI-COR Biosciences	926-32214	1:5000
Donkey anti-mouse IRDye® 680RD	LI-COR Biosciences	926-68072	1:5000

Primer Sequences

qRT-PCR Primer Sequences		
Target	**Forward Primer Sequence (5' to 3')**	**Reverse Primer Sequence (5' to 3')**
EFNB1	GTATCCTGGAGCTCCCTCAACC	GTAGTACTCATAGGGCCGCC
PAX6	TCGGTGGTGTCTTTGTCAACG	ACTACCACCGATTGCCCTGG
GAPDH	TCTTCACCACCATGGAGAAGG	CATGGATGACCTTGGCCAGG
EFNB2	AATCCAGGTTCTAGCACAGACG	GTGCTTCCTGTGTCTCCTCC
EPHB2	CCATCAAGCTCTACTGTAACGGG	GCTCTGTAGTAGCCATTGCG
EPHB3	TGGGTAACATCTGAGTTGGC	CTTGAGCTCCACGTAGACCC
Plasmid PCR Primer Sequences		
Target	**Forward Primer Sequence (5' to 3')**	**Reverse Primer Sequence (5' to 3')**
EBNA-1	ATCAGGGCCAAGACATAGAGATG	GCCAATGCAACTTGGACGTT
GAPDH	ACCACAGTCCATGCCATCAC	TCCACCACCCTGTTGCTGTA

Supplemental References

Neely, M.D., Litt, M.J., Tidball, A.M., Li, G.G., Aboud, A.A., Hopkins, C.R., Chamberlin, R., Hong, C.C., Ess, K.C., Bowman, A.B., 2012. DMH1, a Highly Selective Small Molecule BMP Inhibitor Promotes Neurogenesis of hiPSCs: Comparison of PAX6 and SOX1 Expression during Neural Induction. ACS Chem. Neurosci. 3, 482–491. doi:10.1021/cn300029t

Watanabe, K., Ueno, M., Kamiya, D., Nishiyama, A., Matsumura, M., Wataya, T., Takahashi, J.B., Nishikawa, S., Nishikawa, S., Muguruma, K., Sasai, Y., 2007. A ROCK inhibitor permits survival of dissociated human embryonic stem cells. Nat. Biotechnol. 25, 681–686. doi:10.1038/nbt1310